Localized states in a film-dragging experiment

F. Melo*
Laboratoire de Physique de l'Ecole Normale Supérieure de Lyon, 46, Allée d'Italie, 69364 Lyon, CEDEX 07, France
(Received 19 March 1993)

When a viscous fluid is dragged up the retreating wall of a partially filled cylinder, rotating horizontally, a localized structure can occur corresponding to the spatial coexistence of two different states of the viscous layer. By changing two control parameters, the angular velocity and the amount of fluid, we were able to characterize the domains of stability of coexisting states. Localized structures are stable and stationary in a small region of parameter space where the transition between these two states is large. In analogy with a phase transition with a conserved order parameter, it is suggested that the size of the localized structure is selected from both a law of conservation of total volume of liquid in the cylinder and a stability criterion. By studying the profile and the dynamics of disturbances of the viscous layer, we have shown that both states are well described by the lubrication approximation, but this approximation fails to explain the coexistence of the states.

PACS number(s): 47.52.+j, 47.20.Ma

I. INTRODUCTION

A problem of current interest is pattern formation in nonlinear dissipative systems driven far from equilibrium by an external force. One of the simplest spatial patterns is a localized structure, consisting of two spatially homogeneous stable states coexisting in an interval range of the control parameter. Such localized structures are widely observed experimentally. Well-known examples are local regions of turbulent motion surrounded by laminar flow, which appear in many open flow experiments [1], and spatially localized traveling waves observed at the onset of convection in binary fluid mixtures [2,3].

The central questions of the field concern the mechanism responsible for the stabilization of localized structures and for the selection of their size. Thual and Fauve [4,5] have reported the existence of localized structures in the vicinity of an inverted Hopf bifurcation. They have shown that the stabilization mechanism is a nonvariational effect, i.e., it is due to the absence of a free energy to minimize in the instability problem that they considered.

In contrast, we report, in this paper, the experimental observation of a localized structure associated with a conserved-order-parameter transition. This type of transition is well documented for systems at thermodynamic equilibrium, when the stability and the proportion of coexisting states can be calculated variationally by minimizing the total free energy, while constraining a global quantity to be constant [6]. We present an experimental study of a dissipative system, where a spatially extended layer of viscous fluid breaks into two states above a critical velocity threshold. In the experiment, the viscous fluid is dragged up the inner wall of a horizontally rotating cylinder. At small rotation rates the fluid covers the entire inner surface of the cylinder. However, the coverage is not uniform in the azimuthal direction and a bump is formed near the bottom of the cylinder. This bump shows a well-defined and perfectly horizontal front parallel with the principal axis of the cylinder (the z axis) [see Fig. 1(b)]. At high rotation rates the coverage is completely uniform; the bump disappears [see Fig. 1(a)]. At intermediate rotation rates these two regions of coverage coexist along the z axis. Below the onset of the coexistence state, the dragging of fluid is homogeneous in the axial direction, but when the rotation velocity is increased further, we observe the fragmentation of the layer into three regions: two lateral regions of completely uniform azimuthal coverage surrounding a central region of nonuniform coverage (see Fig. 4). The borders between any two regions connect in space the two possible homogeneous solutions (along the z axis) and correspond to kink-type defects. We observe that the size of the central region, which we call a localized structure, decreases when the angular velocity is increased. We show experimentally that the size of the localized structure is determined by both the total conservation of fluid in the cylinder and the limits of stability of each state. This behavior is similar to the classical thermodynamic phase coexistence when a global quantity is conserved. The dynamics and stability of the two states is studied in detail. Each state is characterized by measuring its profile and by studying the dynamics of imposed disturbances. It is shown that the lubrication approximation [7] explains the main features of the observed behavior but fails to explain the coexistence between the states: in this approximation a continuous transition is expected.

This paper is divided into four sections. In Sec. II we

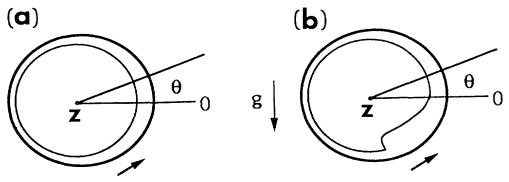

FIG. 1. Sketch of the profile of the film on the inner surface of the horizontal cylinder: (a) Homogeneous film state; (b) flat front state. (The z axis is perpendicular to the plane of the figure and is superposed with the principal axis of the cylinder.)

describe the experiment itself, investigate the global behavior of the system, and present our primary experimental results, namely, a brief description of the observed behavior and a phase diagram.

In Sec. III we summarize the lubrication approximation for the viscous layer, extend it, and discuss how it applies to our experiment by comparing with more refined experimental results: the measurement of the profile and a study of the dynamics of disturbances of the viscous layer. The main features of the profile and the dynamics of disturbances are in good agreement with the lubrication approximation. However, this theory fails to explain the coexistence between the states. Further, we present measurements of the size of localized structures and perform a quantitative analysis utilizing both the global conservation of volume and the stability criterion for coexisting states. Finally, in Sec. IV a short conclusion is given.

II. THE EXPERIMENT

Our experimental setup consists of a horizontal rotating cylinder of inner radius 5 cm and length 56 cm, driven by a variable-speed motor at a rotation frequency in the range 0.1–3.0 Hz, with velocity fluctuations less than 2%. Vibrations produced by the motor are damped by the coupling with the cylinder, and deviations of the cylinder's principal axis from the horizontal are less than 5×10^{-4} rad. The cylinder is made of glass and was rectified to reduce the variation of its inner radius to less than 1%.

The two main experimental parameters are the volume of fluid per unit length, i.e., the area of the cross section of the cylinder occupied by the fluid, A, and the angular velocity ω. We consider only the case $A \ll A_T$, where A_T is the total inner cross section of the cylinder. Various regimes can be observed depending on these parameters and properties of the fluid [7–12]. The behavior we describe here was observed using a silicon oil (Rhodorsil 47V500), with kinematic viscosity $\nu=5$ cm^2 s^{-1}, surface tension $\gamma=21$ erg/cm^2 at 25 °C, and density $\rho=0.97$ g/cm^3. This oil ensures a perfect wetting of the glass substrate.

For high enough angular velocity, all the fluid gets dragged up the inner wall of the cylinder, forming a nearly uniform stationary film. We call this state a "homogeneous film state" [see Fig. 1(a)]. In contrast, if the angular velocity is small enough, a part of the liquid remains near the bottom of the cylinder and generates a bump. The bump is parallel with the principal axis of the cylinder, and its steep part can be seen as a flat front. We call this state the "flat front state" [see Fig. 1(b)]. The front is stationary in the frame of the laboratory and perfectly horizontal [see Fig. 3(a)]. The transition between the homogeneous film and the flat front states is not continuous, and several situations, depending on whether ω is increased or decreased, are observed.

We first studied the existence domain of the homogeneous film state. When ω is decreased, the homogeneous film becomes unstable at a critical velocity $\omega_{c2}(A)$. At the threshold, it starts to develop small localized disturbances that correspond to a local excess of fluid traveling azimuthally on the free surface of the film. Their velocities depend on angular position θ (θ is defined from the horizontal; see Fig. 1) and on the rotation rate: the disturbances are observed to travel slowly near $\theta=0$ and quickly near $\theta=\pi$.

In order to measure the onset of instability, we very slowly decrease the angular velocity in small steps. After each step, we wait for a time on the order of 30 periods of rotation. It was observed that this time is larger that the time necessary to reach a stationary regime. In this way, we obtain the critical velocity $\omega_{c2}(A)$, and by measuring it for several values of A, we obtain the limit of stability of the homogeneous film. The experimental results are presented in the phase diagram in the space of ω and A^2 (see Fig. 2). The dependence of $\omega_{c2}(A)$ with A^2 is linear, and the best resulting fit is the solid line ω_{c2} in Fig. 2.

When ω is decreased further and reaches a second critical velocity $\omega_{c0}(A)$, the velocity of the disturbances vanishes near $\theta=0$; several disturbances can collapse together and stop at the same horizontal position, where they create localized bumps. The bumps are organized in an aperiodic pattern, as shown in Fig. 3(c). The profile of bumps is smooth if A is small and steep if A is large [see Fig. 3(c)]. Their axial size is about 1 cm. This transition was measured and the experimental results correspond to the straight line ω_{c0} on the phase diagram of Fig. 2. The bumps expand laterally as soon as ω is decreased. When ω reaches a new critical velocity $\omega_{c1}(A)$, they collapse together forming a horizontal flat front. This transition was also measured and the experimental results plotted in the phase diagram. The dependence of $\omega_{c1}(A)$ with A^2 is also linear, and the best resulting fit is the solid line ω_{c1} in Fig. 2. We note that when A is small enough, the transition between the homogeneous film and the flat front

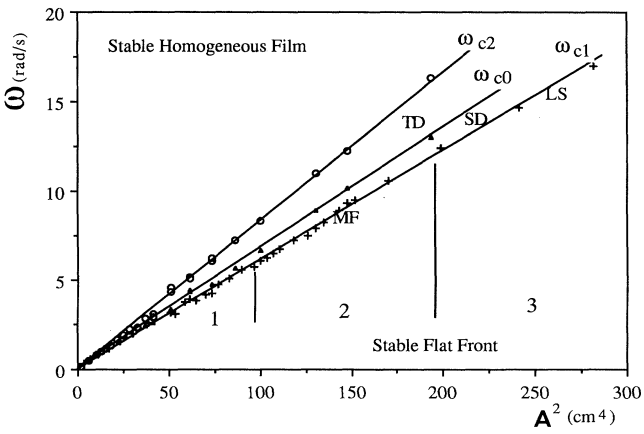

FIG. 2. Phase diagram in the plane (ω, A^2). In the region TD we observe traveling disturbances, in SD, stationary disturbances. The threshold for transitions undergone by the flat front is given by the line ω_{c1}; for values of A in region 2, the transition is to a modulated front (MF). In region 3, the transition is to localized structures (LS).

states is roughly continuous. Experimentally, it becomes difficult to differentiate between ω_{c1}, ω_{c0}, or ω_{c2}: the disturbances appear preferentially near $\theta=0$ and remain there where they collapse together laterally and form rapidly into a bump along the principal axis of the cylinder. Moreover, the profile of the bump along the cylinder is smooth so that the front is not well defined.

In the following, we study how the flat front state destabilizes when the angular velocity is increased. For small angular velocity the front is straight in the axial direction except near the lateral walls where the boundary creates small dips. At the threshold the front destabilizes and disappears in different ways depending on A. Three cases can be distinguished.

For small A, the bump disappears gradually: the fluid contained in the bump is slowly and homogeneously redistributed along the circumference of the cylinder. Nevertheless, it creates small traveling disturbances on the film. Later, these disturbances are damped to give rise to a homogeneous film state.

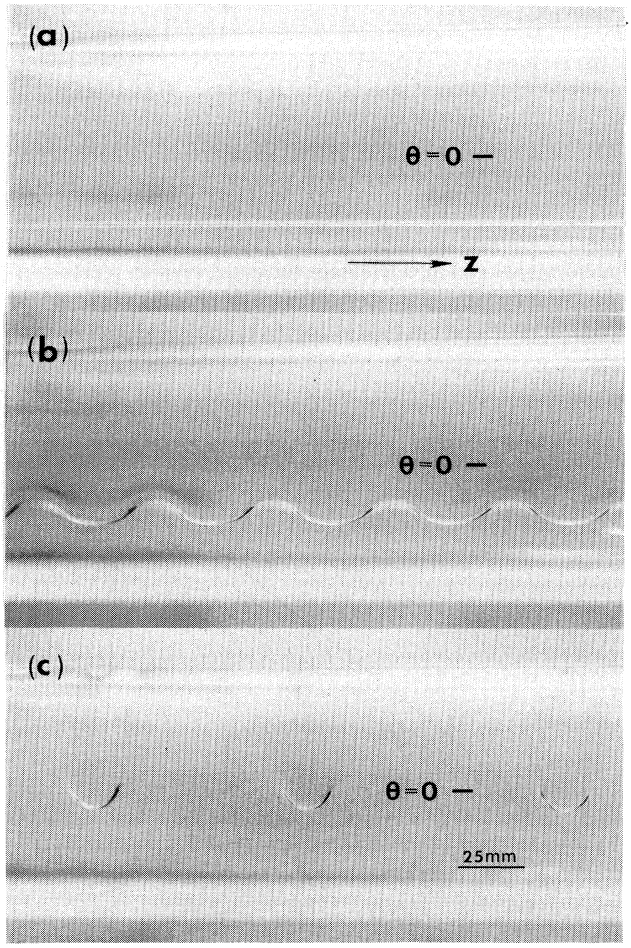

FIG. 3. Photographs of fronts in the cases of (a) $\omega=6.9$ rad/s, a stable flat front; (b) $\omega=7.3$ rad/s, a stationary wavy front; (c) $\omega=7.5$ rad/s, a quasiperiodic pattern of bumps. $A=10.7$ cm^2. The dashes indicate the $\theta=0$ location in the cylinder.

For intermediate A, the linear front becomes wavy in the z direction [cf. Fig. 3(b)]. It takes on a sinusoidal shape of well-selected wavelength but the transient is long: on the order of the viscous diffusion time over the length of the front ($\tau\sim L^2/\nu$). The wavelength of the pattern is about 5 cm and practically independent of A. The amplitude of the sinusoid is discontinuous at the threshold and increases quickly with angular velocity. The bifurcation is thus a first-order transition and the observed critical angular velocity is proportional to A^2. For all the volumes that we investigate, the pattern is regular but is stable only very close to the instability threshold; when ω is increased slightly further, the fluid contained in the modulated bump is dragged up the retreating wall. But in this case the dragging is not gradual. It starts in the highest parts of the modulated bump and gives rise to a periodic pattern of drops. These drops are quickly dragged also, but the disturbances that they generate on the films are not damped. In fact, two neighboring disturbances can collapse together and become a stationary, localized bump near $\theta=0$ [cf. Fig. 3(c)]. The profile of bumps is steep and their size is about 1 cm. Frequently, these bumps organize themselves in an aperiodic pattern

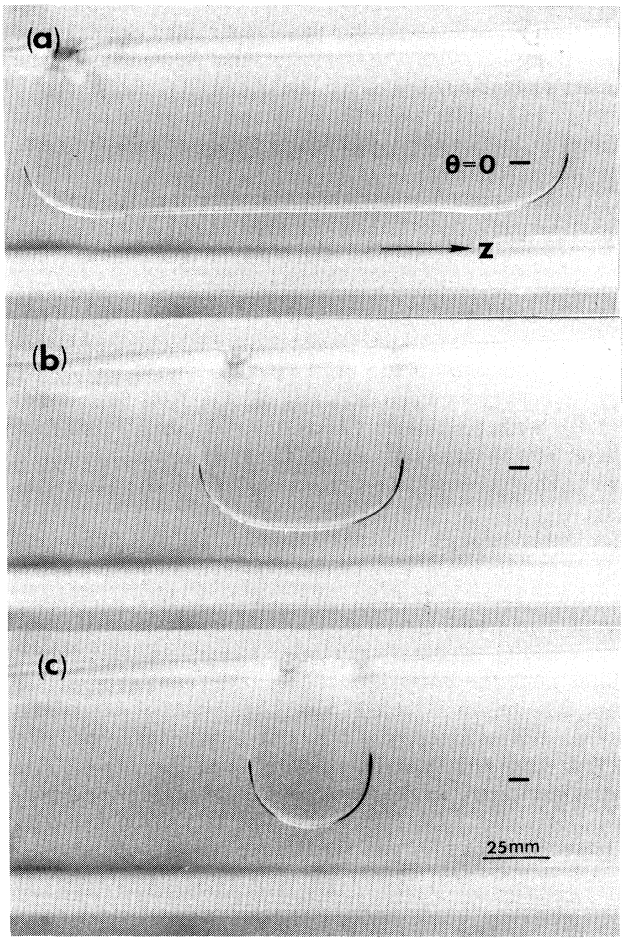

FIG. 4. Localized structure: (a) $\omega=12.1$ rad/s; (b) $\omega=13.06$ rad/s; (c) $\omega=14.45$ rad/s. $A=14.3$ cm^2. The dashes indicate the $\theta=0$ location in the cylinder.

whose mean wavelength is larger than that of the periodic pattern.

Karweit and Corrsin [8] reported a similar pattern formation, also in a horizontal rotating cylinder, but utilizing fluids of small viscosities. In that case, for large rotation rates, most of the fluid still lies at the bottom of the cylinder and the free surface of fluid is quite irregular.

For large A, the front does not disappear completely, but rather we observe that a homogeneous film state and a flat front state coexist at different z locations in the cylinder. At $\omega<\omega_{c1}(A)$, the homogeneous front state exists everywhere, but at the threshold, two small regions of the homogeneous film state start to appear near the lateral walls of the cylinder [cf. Figs. 4(a) and 4(b)]. The central portion of the cylinder remains occupied by the flat front state. We define a localized structure as a region of the flat front state surrounded by the homogeneous film state.

When ω is increased in small steps, the size of the flat front state decreases slowly and its length stabilizes to a well-defined value for each step in ω. As ω increases, most of the fluid moves laterally and goes into the flat front state where it increases the local value of A. The coexisting states then have different "density of volume," and they can be characterized globally by these quantities, which we call A_1 for the flat front state and A_2 for the homogeneous film state.

Between both states and over a distance on the order of the radius of the cylinder, the front is strongly curved. Near $\theta=0$, it becomes tangential to the principal flow and gives rise to a ring of larger thickness at this axial position (see Fig. 4). This is a wall between the states. This wall connects in space the two possible homogeneous solutions and corresponds to a kink-type defect.

The thresholds for the flat front instabilities were measured by very slowly increasing the angular velocity. At each increment, we waited for a time on the order of the viscous diffusion time. In this way, we obtain the critical velocity, and by measuring it for several values of A, we obtain the limit of stability of the flat front state. The experimental results also collapse onto the straight line $\omega_{c1}(A)$ on the phase diagram (see Fig. 2). This shows that the instability of the flat front state has no appreciable hysteresis.

III. THE MODEL

A. A dimensional argument

In order to summarize our experimental results and gain some physical insight about the observed behavior, we look for the relevant dimensionless control parameters of the system: it is well known that such quantities measure the competition between stabilizing and destabilizing effects at the instability onset.

The parameters of the system are the angular velocity ω, the fluid density ρ, the mean thickness of the viscous layer h_0, the fluid viscosity ν, the surface tension γ, the radius of the cylinder R, and the acceleration of gravity g. With these parameters, we define four independent dimensionless numbers: Re, B, C, and ϵ. The dimensionless parameter Re is a Reynolds number, $\mathrm{Re}=R\omega h_0/\nu$. The dimensionless parameter B is an inverse Bond number, $B=\gamma/\rho g R^2$. $C=\omega^2 R/g$ measures the competition between centrifugal and gravitational force. $\epsilon=h_0/R$ measures the fullness of the cylinder (h_0 and A are related by the condition of conservation of volume). All these dimensionless parameters have a clear physical meaning, and any one of them is a constant along the transitions thresholds. We then define a new dimensionless number $\Lambda=\omega\nu R/gh_0^2=C/\epsilon\,\mathrm{Re}$, which measures the competition between viscous stress and gravity. Writing Λ as a function of A, i.e., $\Lambda=(2\pi)^2\nu R^3\omega/gA^2$, we see that Λ is constant along a straight line in the plane (ω, A^2). Each transition presented in the phase diagram (see Fig. 2) is then characterized by a single value of Λ: $\Lambda_0=1.67$, $\Lambda_1=1.56$, and $\Lambda_2=2.14$ for the straight lines ω_{c0}, ω_{c1}, and ω_{c2}, respectively. This result suggests that competition between viscous stress and the tangential component of gravity is responsible for the observed behavior. However, in order to characterize fully the observed behavior, a second dimensionless number is needed. We choose ϵ because it clearly identifies regions 1, 2, and 3 of the phase diagram. In conclusion, a complete description of the system requires four independent dimensionless numbers, but in our case only two dimensionless numbers are relevant: Λ and ϵ.

B. Lubrication approximation

In order to describe more precisely the homogeneous film state and the flat front state, we follow the enlightening work of Moffatt [7]. In the lubrication approximation, the spreading equation reads

$$\nu\frac{\partial^2 u}{\partial y^2}=g\cos(\theta)\ , \tag{1}$$

where u is the azimuthal component of the velocity in the layer, $g\cos(\theta)$ is the tangetial component of gravitational acceleration, and θ is measured from the horizontal (see Fig. 1). y is the radial coordinate that, in this case, is measured from the inner surface and taken positive when moving toward the center of the cylinder. In Eq. (1), inertia effects have been neglected. A necessary condition for the validity of this approximation is $\mathrm{Re}^*=\omega h_0^2/\nu\ll 1$, where Re^* is the Reynolds number for this problem. Solving Eq. (1) with the relevant boundary conditions, $u=R\omega$ at $y=0$ and $\partial u/\partial y=0$ at $y=h$, Moffatt obtained

$$Q(\theta,t)=h(\theta,t)R\omega-\frac{g\cos(\theta)[h(\theta,t)]^3}{3\nu}\ , \tag{2}$$

where $Q(\theta,t)=\int_0^h u\,dy$ is the flux at the angle θ and h is the local film thickness. The height profile is obtained from the continuity equation

$$\frac{\partial h}{\partial t}+\frac{1}{R}\frac{\partial Q}{\partial\theta}=0\ . \tag{3}$$

Equation (3) arises from volume conservation; for a homogeneous state, its integral form reads

$$A=\int_0^{2\pi} Rh(\theta)d\theta=2\pi Rh_0 \ . \tag{4}$$

Suppose now that the flow has reached steady state, then clearly Q is constant and $h(\theta)$ is given in terms of Q from Eq. (2). This equation is represented graphically in Fig. 5. Here, Q is presented as a function of h for constant ω; θ is used as a continuous parameter. Note that at $\theta=0$, Q has a maximum, $Q_{\max}=\frac{2}{3}R\omega\sqrt{R\omega\nu/g}$, when $h=h_{\max}=\sqrt{R\omega\nu/g}$. A continuous solution for $h(\theta)$ is then given by the intersection of the horizontal line, corresponding to a given value of Q, with the family of curves in Fig. 5. As pointed out by Moffatt, a continuous solution for h then exists if and only if $Q\le Q_{\max}$. In this case, $h(\theta)\le h_{\max}$, since larger values of h cannot be reached continuously. The condition $Q\le Q_{\max}$ for the existence of the continuous solution can be translated, from Eq. (4), into a condition involving the total volume of fluid and the rotation rate, that is, for a given A, ω must not be smaller than a critical value $\omega_c=(A/4.428R)^2g/R\nu$ [7] (this corresponds to $\Lambda=2.06$). Physically, it means that there exists a minimum value of ω for which all the fluid can be dragged up the retreating surface to form a stationary film. In other words, the homogeneous film solution no longer exists if the tangential component of gravity cannot be balanced everywhere by viscous stress. This occurs first near $\theta=0$ when $h=h_{\max}$ so that $Q=Q_{\max}$.

Nevertheless, we think that a stationary solution for which the profile presents a thicker layer bounded by a horizontal discontinuity near the bottom of the cylinder representing the flat front state is also possible if $\omega<\omega_c$. This solution can be obtained by intersecting a horizontal line corresponding to $Q_{\max}$ with the family of curves in Fig. 5, but by taking the values of h larger than $h_{\max}$ in the lower portion of the cylinder. The angular position of the discontinuity can be obtained from conservation of volume of fluid in the cylinder [Eq. (4)]. We note that the resulting profile has a single discontinuity only if Q is equal to $Q_{\max}$. Otherwise, two discontinuities are necessary to reach value of h larger than $h_{\max}$ ($Q<Q_{\max}$) or no solution exists ($Q>Q_{\max}$).

In conclusion, two states for the viscous layer are possible depending on the angular velocity. The transition between states must be continuous: the homogeneous film state becomes a flat front state at ω_c. Thus, the lubrication approximation cannot explain the coexistence domain between these states. This can only be explained by invoking a minimal bump size so that it is necessary to have a finite amount of fluid to build a flat bump. The onset for the flat front state must then be smaller than ω_c. In the following subsections we study experimentally the two states of the system and we discuss how the lubrication approximation applies.

C. The stationary homogeneous film state

In order to describe precisely the homogeneous film state and to check the predictions of the lubrication approximation, we have measured the film thickness "h" as a function of θ for a constant A and several values of ω, all larger than $\omega_{c2}(A)$. The data were taken with a tip gauge positioned directly above the free surface of the film. The film thickness was then measured by the tip gauge, which could be moved in the radial and angular directions with a precision of about 10^{-2} mm and 0.2°, respectively. The experimental results are shown in Fig. 6. The profile of the film varies slowly with θ, having the largest variation for small ω. Experimentally, Q was determined by measuring $h(\pi/2)$, from the relation $Q=h(\pi/2)R\omega$ [14]. The solid lines in Fig. 6 correspond to the intersection of this value with the family of curves in Fig. 5; very good agreement is obtained without any adjustable parameter. It is necessary to note that the hydrostatic pressure contribution (due to the radial component of gravity), the centrifugal force, and the surface tension effect were also neglected in deriving Eq. (2). This assumption is valid if h_0/R, ω^2h_0/g, and $\gamma h_0/\rho gR^3$ are smaller than unity, which is the case in the domain of parameter explored experimentally.

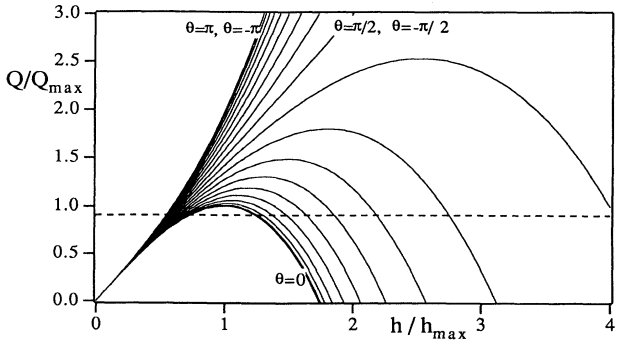

FIG. 5. Geometric representation of Eq. (2). $Q/Q_{\max}$ is presented as a function of $h/h_{\max}$ utilizing θ as a parameter ($Q_{\max}=\frac{2}{3}R\omega\sqrt{R\omega\nu/g}$ and $h_{\max}=\sqrt{R\omega\nu/g}$). When $Q/Q_{\max}<1$, the intersection of the dashed line with the family of curves gives a continuous solution for $h(\theta)$. A solution with a single front is possible only if $Q=Q_{\max}$.

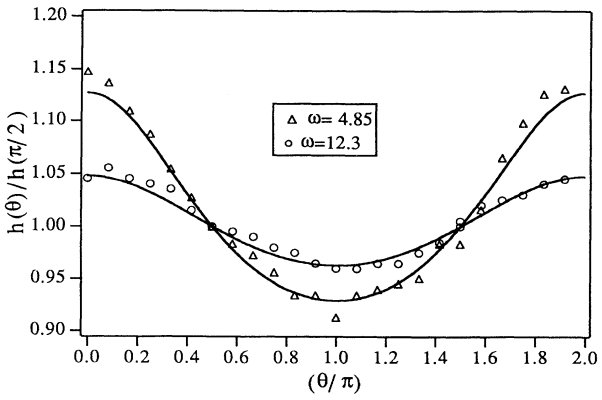

FIG. 6. Profile of the homogeneous film state for various values of ω and $A=6.25$ cm^2. $h(\pi/2)=0.183$ cm for $\omega=4.85$ rad/s, and $h(\pi/2)=0.198$ cm for $\omega=12.3$ rad/s. The solid lines correspond to the theoretical profile obtained from the lubrication approximation.

D. Dynamics and stability of the homogeneous film state

Above ω_{c2} the homogeneous film is observed to be stable, and we can gain physical insight about its dynamics and stability by studying the spatiotemporal evolution of local artificially created disturbances. These were generated by small drops that were released onto the free surface of the film by a pipette. When a disturbance is created, two phenomena are observed. First, it is quickly advected by the flow and, second, it is damped or amplified. The damping or amplification of disturbances depends on angular position. A disturbance crossing the region between $\pi<\theta<2\pi$ (the stabilization region) is slightly damped. In contrast, it is observed that a disturbance is slightly amplified by the radial component of gravity while it crosses the region between $0<\theta<\pi$ (the destabilization region). Despite this, for ω above ω_{c2}, the global result is a damping of disturbances after several revolutions of the cylinder. Note that the characteristic time of amplification of a disturbance of size l near $\theta=\pi/2$ is $\tau_D \sim 3\nu l^2/gh_0^3$ and that the characteristic time of advection of a disturbance is $\tau_A \sim \pi/\omega$. Thus, when ω is decreased, a disturbance crossing the destabilization region in a time τ_A larger than τ_D could be considerably amplified and the homogeneous film could become unstable. Taking $l \sim 10 l_c$ ($l_c=\sqrt{\gamma/\rho g}$ is the capillary length), which is the size of disturbance observed experimentally, we find that, at the threshold and for the domain of parameters explored experimentally, τ_A is always smaller than τ_D. This estimate shows that the amplification effect is not responsible for the instability of the homogeneous film; the stabilizing effects of surface tension, centrifugal force, and the radial component of gravity (in the stabilization region) dominate. In fact, in the destabilization region the homogeneous film state must be unstable to the Rayleigh-Taylor instability [13]. This phenomenon was not observed because the disturbances are quickly advected, passing out of the destabilization region before they actually grow.

As discussed earlier, in the framework of the lubrication approximation, the homogeneous film solution no longer exists if ω is smaller than the critical value

$$\omega_c=(A/4.428R)^2 g/R\nu .$$

The experimental results presented in Fig. 2 show that ω_{c2} is proportional to A^2 with the constant of proportionality nearly equal to the value predicted by the lubrication approximation. The instability of the homogeneous film state is then due to the tangential component of gravity, which cannot be balanced by viscous stress near $\theta=0$. At the threshold, the fluid which cannot be dragged accumulates near $\theta=0$ where it forms small disturbances. As we pointed out in Sec. II, at the threshold and for small A disturbances were observed effectively to stop near $\theta=0$. When A is large, the disturbances do not stop. This is not surprising because ω_{c2} increases with A so that a disturbance can have enough kinetic energy to cross the region where viscous stress vanishes.

In the following we measure the azimuthal velocity of the artificial disturbances. We consider the case of small A only. The velocities were measured by a differential position photosensor placed very near the free surface of the film. It detected the time of transit of a disturbance between the two sensing points of the photosensor, which were illuminated homogeneously by a planar laser beam. Then, in the absence of disturbances, the sensing points remain homogeneously illuminated, giving a very small signal. A disturbance passing in front of the sensor deviates light from the laser, giving two opposite peaks whose time delay is measured by a numeric oscilloscope. In Fig. 7 we show the mean velocity of disturbances ω_p, for $\theta=0$ and π, as a function of local thickness h and for a constant ω (h is varied by changing A). At $\theta=0$, ω_p/ω remains nearly 1 as long as $h \ll h_c$ (h_c is defined at $\omega=\omega_{c2}$), it decreases with increasing h, and becomes practically zero when h reaches h_c; the disturbances stop near $\theta=0$. At $\theta=\pi$, ω_p/ω always increases with h.

A straightforward estimation of the velocity of localized disturbances can be obtained from a linear stability analysis of Eq. (3). The resulting equation, which gives the dynamics of disturbances, includes an advection term of the form

$$\frac{\omega_p}{\omega}=1-\frac{g\cos(\theta)h^2}{R\nu\omega} , \tag{5}$$

where ω_p is the advection velocity and h is the nonperturbed profile. This relation is represented by the solid lines in Fig. 7 for $\theta=0$ and π. The agreement with experimental results is good considering that there is no adjustable parameter. Therefore, we think that the advection of disturbances is well characterized by this term. We do not suggest that the dynamics of local disturbances is given by a simple equation of advection, but rather that the advection phenomenon can be isolated from the diffusion phenomenon when the time scale is small enough. We think that this is the case when we measure a local velocity.

The variation of ω_p/ω with θ was studied in more detail by measuring ω_p/ω as a function of θ for two values of ω and constant A. The experimental results plotted in the inset of Fig. 7 show that for values of θ in the interval

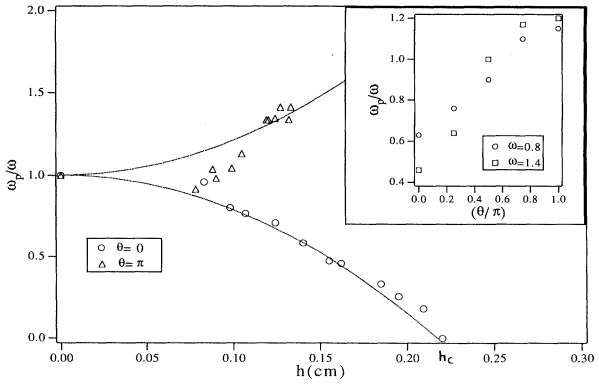

FIG. 7. Local tangential velocity ω_P of disturbances normalized to ω as a function of h. $\omega=1.85$ rad/s. The inset shows ω_P as a function of θ: $A=2.5$ cm^2; $\omega_{c2} \sim 0.5$ rad/s.

$[\pi/2, 3\pi/2]$, ω_p/ω is always of order unity and slowly increasing when ω is decreased. A larger decrease of ω_p/ω is observed for θ in the interval $[-\pi/2, \pi/2]$. As a result of the variation of ω_p/ω with θ, focusing and defocusing effects appear. To explain these effects, we consider two disturbances starting at different angular positions, the first one at some θ_1 near the center of the interval $(3\pi/2, 2\pi)$ and the second one at θ_2 near the center of the interval $(\pi, 3\pi/2)$. The two disturbances approach $\theta=0$ with decreasing velocities. As the velocity of the second one is larger, the distance between disturbances decreases; this is the focusing effect, which is equivalent to what occurs when two cars start to slow down at a red light. Alternately, when the first disturbance crosses $\theta=0$, its velocity starts to increase, while the velocity of the second one is still decreasing. The distance between the two disturbances then increases; this is the defocusing effect.

E. The flat front state

In this section we describe the evolution of the flat front state with rotation rate, before its destabilization. We measured the thickness of the film at $\theta=\pi/2$ as a function of ω for several values of A. The experimental results (see Fig. 8) show that $h(\pi/2)$ varies as $\sqrt{\omega}$ and does not depend on the value of A; all the experimental data collapse onto a single curve. This result is in agreement with the lubrication approximation, where the scale of h is given by $h(\pi/2) \propto \sqrt{R\omega\nu/g}$. Moreover, in the particular case, when the flux is equal to $Q_{\max}$, Eq. (2) predicts that $h(\pi/2)=\frac{2}{3}\sqrt{R\omega\nu/g}$. This law is represented by the solid line in Fig. 8. Because all the experimental data collapse onto this particular curve, we conclude that in the flat front state, Q is always close to $Q_{\max}$. This result is independent of A. The inner wall of the cylinder is then dragging the maximal quantity of liquid predicted by the lubrication approximation.

Next, we measured the profile of the flat front state. Two cases are distinguished: small and large A. For small A, Fig. 9(a) shows the profile of the front state for

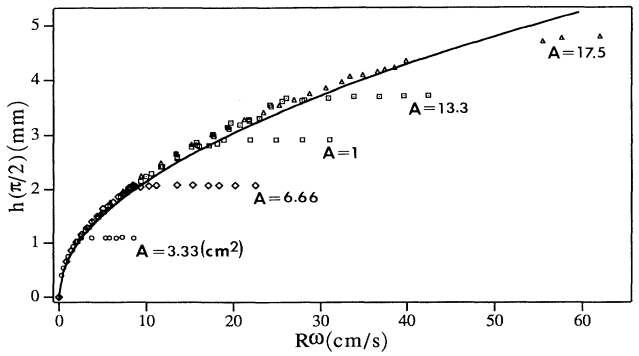

FIG. 8. Thickness of film at $\theta=\pi/2$ as a function of ω and several values of A. In the flat front regime, $h(\pi/2)$ is independent of A and is proportional to $\sqrt{\omega}$. The experimental value of the numerical constant of proportionality shows that the flux traversing the angular section at $\theta=\pi/2$ is always close to the maximum value predicted by the lubrication approximation.

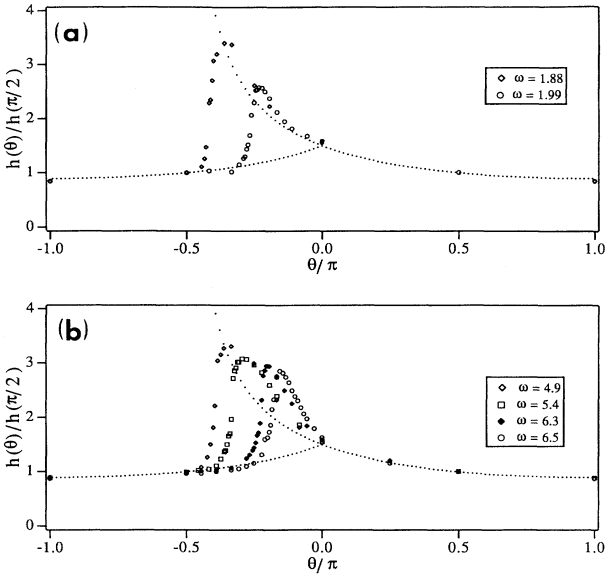

FIG. 9. Profile of the linear front state for various values of ω: (a) $A=6.25$ cm^2. When $h(\theta)$ is normalized to $h(\pi/2)$, the profile of the film scales as $\sqrt{\omega}$. The dotted lines correspond to the two theoretical branches obtained in the lubrication approximation. (b) $A=10.2$ cm^2. In the bump, experimental results deviate from the prediction of the lubrication approximation. Close to the steep-slope part, other effects must be taken into account [15]. The units of ω are rad/s.

two values of ω. The bump near the bottom of the cylinder and a slowly varying part elsewhere. The bump has a smooth part which matches tangentially, near $\theta=0$, with the slowly varying part, and a steep slope part, defining a front. We show that when $h(\theta)$ is normalized to $h(\pi/2)$, experimental profiles collapse into a single shape, except near the steep-slope part of the bump. When ω is increased, this part of the bump moves to larger θ values as a result of the decrease in the amount of liquid in the bump. These results show that the profile of the linear front state scales as $\sqrt{\omega}$. Moreover, the profile of the linear front state follows the form predicted by the lubrication approximation when $Q=Q_{\max}$ and is represented by the dashed lines in Fig. 9(a).

For large A, the results plotted in Fig. 9(b) are similar, but the profile of the bump does not scale as $\sqrt{\omega}$ anymore. The nondimensional slope of the smooth part of the bump increases with ω. Nevertheless, we think that the profile of the linear front state is not physically different from the second solution given by the lubrication approximation. The observed deviations are probably due to surface tension and to the inertial and geometric effects [15] which become important when the thickness of the bump becomes large.

F. Localized structure

In the nucleation of localized structures, two situations are possible: the viscous layer can break into several localized structures or form a single one, depending on the way in which the rotation rate is increased to reach the

coexistence domain. We first study the case of a single localized structure. The density of volume is identified as the naturally conserved order parameter whose global conservation reads

$$LA=\lambda A_1+(L-\lambda)A_2 , \tag{6}$$

where λ is the size of the isolated localized structure and L is the length of the cylinder. Let us assume that A_1 and A_2 are given by the limit of stability of each state (presented in the phase diagram of Fig. 1). Then from Eq. (6) we can write the following relation for the evolution of λ with ω:

$$\frac{\lambda}{L}=\left[\frac{A}{\sqrt{\omega}}-\frac{1}{\sqrt{\alpha_2}}\right]\left[\frac{1}{\sqrt{\alpha_1}}-\frac{1}{\sqrt{\alpha_2}}\right]^{-1} , \tag{7}$$

where α_1 and α_2 are the slope of the lines ω_{c1} and ω_{c2} respectively, in the phase diagram of Fig. 2 ($\alpha_1=6.15\times10^{-2}$ and $\alpha_2=8.5\times10^{-2}$ rad s^{-1} cm^{-4}). The last assumption appears justified because the coexisting states were observed to be sensitive to perturbations. For example, when ω was increased by a small jump, the flat front state broke into several localized structures. Equally, small bumps appeared spontaneously on the portions of homogeneous film. This shows that both states are close to their limits of stability. Thus, A_2 and A_1 are given reasonably well by the lines ω_{c2} and ω_{c1} of the phase diagram.

In order to measure λ as a function of ω, we increased the angular velocity very slowly and at each increment we waited a time of at least order τ. In this way only one localized structure appears in the central region of the cylinder. The experimental results are plotted in Fig. 10. When λ is of order L, its evolution with ω is well described by Eq. (7). However, when λ becomes small, Eq. (7) predicts a value smaller than the value observed experimentally. We think that in the latter case, λ is dominated by the repulsive interaction between the two walls of the localized structure, rather than by a marginal stability criterion.

When our system was quenched in the coexistence region by a jump of angular velocity, the viscous layer broke into several localized structures of different sizes. The total length occupied by these structures decreased faster than the prediction of Eq. (7) (see Fig. 10). We think this is due to the finite amount of fluid contained in the walls of the localized structure. Equation (7) must then be corrected to take this effect into account. Moreover, this effect becomes dominant when the number of walls is large.

In our experiment the formation of localized structures is seen to be similar to the formation of droplets in a phase transition with a conserved order parameter. For instance, when an impurity-containing substance at the solid-liquid transition is quenched in the coexistence domain, it breaks in two phases. Many small regions of a solid phase, low in impurities, then appear. We can also imagine a small system where only one region nucleates. In both cases the global conservation of impurities controls the final state of the system. In the first case, it gives the volume occupied by the collection of regions and in the second case it controls the size of the single region.

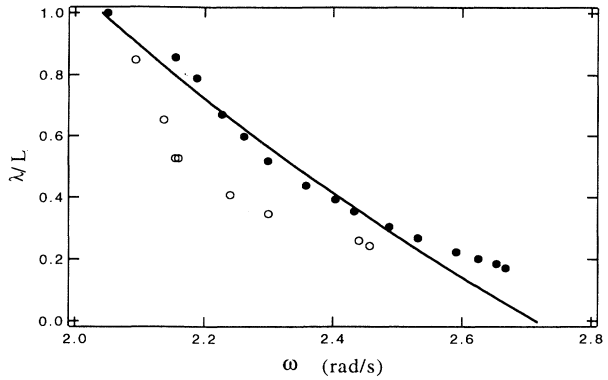

FIG. 10. λ/L as a function of ω, for $A=14.3$ cm^2. The solid line represents the prediction of Eq. (7). The closed circles correspond to the size of a single localized state; the open circles correspond to the total size of several localized states.

IV. CONCLUSION

We have shown that two states of the viscous layer can coexist and give rise to localized structures. By extending the model of Ref. [7], we are able to explain the general features of the coexisting states, namely, their profiles and the dynamics of imposed disturbances. Nevertheless, this model cannot explain the coexistence of the states because it predicts a continuous transition between them. This coexistence can only be explained by invoking a minimal bump size, so that a finite amount of fluid is necessary to build a flat bump. Thus, the onset for the flat front state is smaller than ω_c, as was observed experimentally.

In Sec. III, we have seen that the size of a single localized structure is well described by both global conservation and by stability arguments for coexisting states. Thus, the transition from the flat front state to a localized structure appears as the nonequilibrium analog of a thermodynamic transition with conserved order parameter. In such a transition, the stability and the proportion of the coexisting state can be calculated variationally by minimizing the total free energy while constraining a global quantity to be constant. However, this has not been done in our system since, as yet, no expression for the free energy has been found.

ACKNOWLEDGMENTS

I am very grateful to Ch. Baudet, S. Douady, J. F. Pinton, and P. Umbanhowar for helpful suggestions.

*Present address: Center for Non-Linear Dynamics, University of Texas, Austin, TX 78712.

[1] D. J. Tritton, *Physical Fluid Dynamics* (Van Nostrand Reinhold, New York, 1977), Chap. 19.
[2] E. Moses, J. Fineberg, and V. Steinberg, Phys. Rev. A **35**, 2757 (1987).
[3] R. Heinrichs, G. Ahlers, and D. S. Cannel, Phys. Rev. A **35**, 2761 (1987).
[4] O. Thual and S. Fauve, J. Phys. (Paris) **49**, 1829 (1988).
[5] S. Fauve and O. Thual, Phys. Rev. Lett. **64**, 282 (1990).
[6] See, for instance, Ph. Nozières, *Transitions à l'Equilibre Thermodynamique* (Cours au Collège de France, Paris, 1989).
[7] H. K. Moffatt, J. Mec. **16**, 651 (1977).
[8] M. J. Karweit and S. Corrsin, Phys. Fluids **18**, 111 (1975).
[9] F. M. Orr and L. E. Scriven, J. Fluid Mech. **84**, 145 (1978).
[10] T. Brooke Benjamin and S. K. Pathak, J. Fluid Mech. **183**, 399 (1987).
[11] D. D. Joseph and L. Preziosi, J. Fluid Mech. **185**, 323 (1987).
[12] L. Preziosi and D. D. Joseph, J. Fluid Mech. **187**, 99 (1988).
[13] G. Taylor, Proc. R. Soc. London Ser. A **201**, 192 (1950).
[14] At $\theta=\pi/2$, the tangential velocity of the fluid is $R\omega$. Because this result does not depend on centrifugal force and inertial effects, the measurements of $h(\pi/2)$ must give a good estimation of Q.
[15] The lubrication approximation may break down at the bump where $\partial h/\partial\theta$ can become large. In that case, new terms due to the cylindrical geometry must be taken into account in Eq. (2).

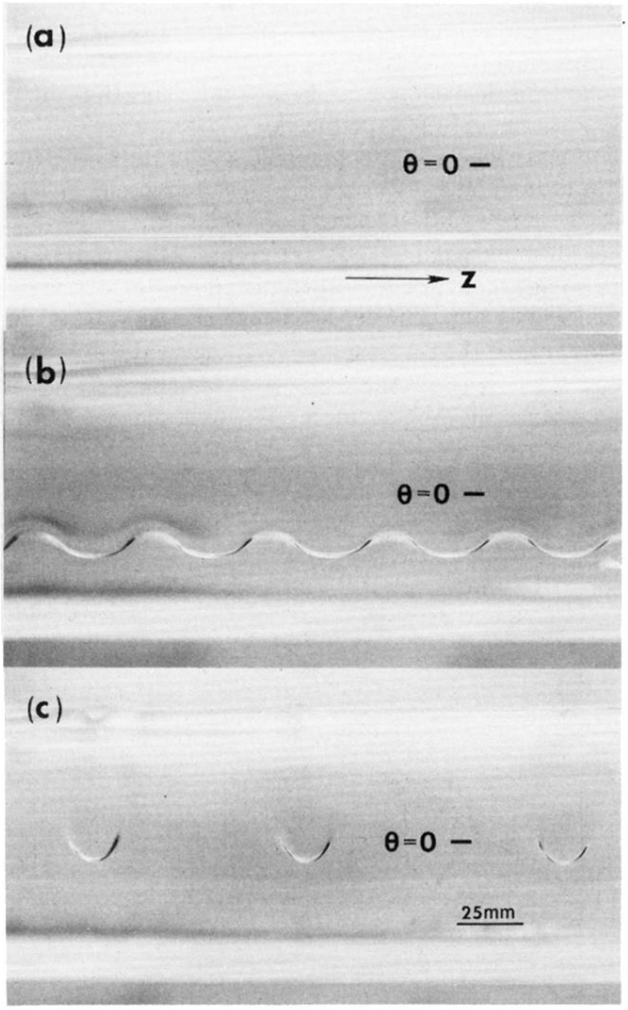

FIG. 3. Photographs of fronts in the cases of (a) $\omega=6.9$ rad/s, a stable flat front; (b) $\omega=7.3$ rad/s, a stationary wavy front; (c) $\omega=7.5$ rad/s, a quasiperiodic pattern of bumps. $A=10.7$ cm^2. The dashes indicate the $\theta=0$ location in the cylinder.

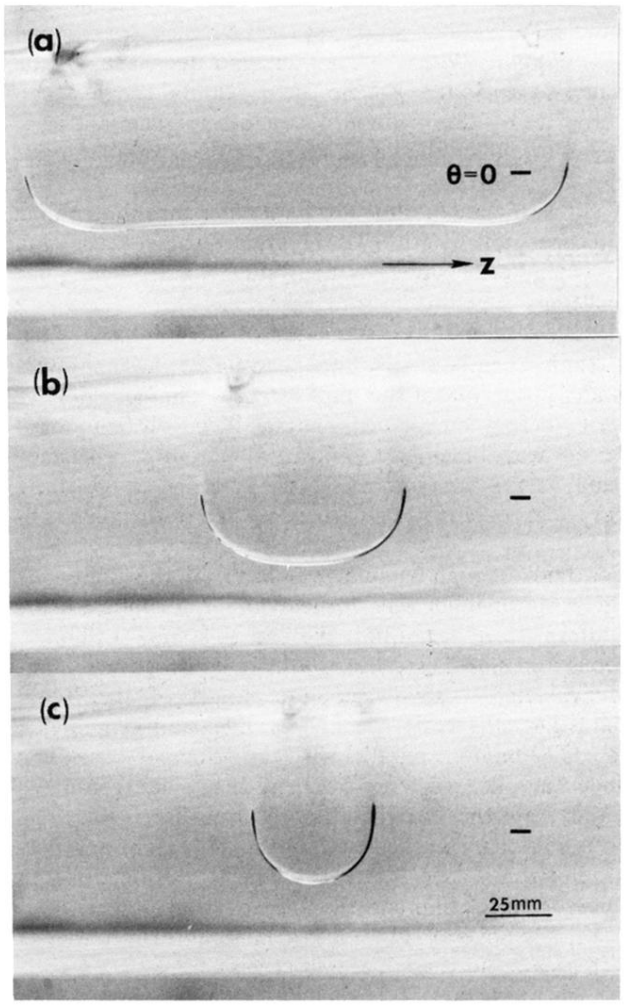

FIG. 4. Localized structure: (a) $\omega = 12.1$ rad/s; (b) $\omega = 13.06$ rad/s; (c) $\omega = 14.45$ rad/s. $A = 14.3$ cm^2. The dashes indicate the $\theta = 0$ location in the cylinder.